Hydrology and
Earth System
Sciences
Discussions

1 # SMPD: A soil moisture-based precipitation downscaling method for

2 # high-resolution daily satellite precipitation estimation

3 Kunlong He[1,2], Wei Zhao[1, *], Luca Brocca[3], Pere Quintana-Seguí[4]

4 [1]Institute of Mountain Hazards and Environment, Chinese Academy of Sciences, Chengdu 610041, China

5 [2]School of Energy and Power Engineering, Xihua University, Chengdu 610039, Sichuan, China;

6 [3]Research Institute for Geo-Hydrological Protection, National Research Council, Perugia, Italy

7 [4]Ebro Observatory (OE), Ramon Llull University – CSIC, Roquetes, Spain.

8 *Correspondence*: Wei Zhao (zhaow@imde.ac.cn)

9 **Abstract.** As a key component in the water and energy cycle, precipitation with high resolution and accuracy is of great

10 significance for hydrological, meteorological, and ecological studies. However, current satellite-based precipitation products

11 have a coarse spatial resolution (from 10 to 50 km) not meeting the needs of several applications (e.g., flash floods and

12 landslides). The implementation of spatial downscaling methods can be a suitable approach to overcome this shortcoming. In

13 this study, we developed a Soil Moisture-based Precipitation Downscaling (SMPD) method for spatially downscaling the

14 Integrated Multi-satellitE Retrievals for GPM (IMERG) V06B daily precipitation product over a complex topographic and

15 climatic area in southwestern Europe (Iberia Peninsula), in the period 2016-2018. By exploiting the soil water balance equation,

16 high-resolution surface soil moisture (SSM) and Normalized Difference Vegetation Index (NDVI) products were used as

17 auxiliary variables. The spatial resolution of the IMERG daily precipitation product was downscaled from 10 km to 1 km. An

18 evaluation using 1027 rain gauge stations highlighted the good performance of the downscaled 1 km IMERG product compared

19 to the original 10 km product, with a correlation coefficient of 0.61, root mean square error (RMSE) of 4.83 mm and a relative

20 bias of 5%. Meanwhile, the 1 km downscaled results can also capture the typical temporal and spatial variation behaviours of

21 precipitation in the study area during dry and wet seasons. Overall, the SMPD method greatly improves the spatial details of

22 the original 10 km IMERG product with also a slight enhancement of the accuracy. It shows good potential to be applied for

23 the development of high quality and high-resolution precipitation products in any region of interest.

24

25 **Keywords:** GPM; SMPD; surface soil moisture; spatial downscaling; daily precipitation

26

1 Introduction

Precipitation, as a key driving force of the global water cycle under climate change conditions, changes greatly in space and time and is among the key factors affecting the hydrology, water resources and ecosystem of a watershed (Salzmann, 2016; Spötl et al., 2021). Hence, accurate and reliable spatial-temporal precipitation estimates are critical for the assessment and understanding of climate change, hydrology, climatology, and its impacts on the environment, ecosystem, and human society (Ma et al., 2021; Wehbe et al., 2020; Xia et al., 2015; Bezak et al., 2021; Wei et al., 2020; Yang and Huang, 2021).

The most common ground-based method for precipitation measurement relies on rain gauge observations. Although rain gauges can provide accurate observations and capture the temporal variability in precipitation within a certain radius, these measurements are known to be prone to spatial representativeness issues due to the high spatiotemporal heterogeneity of precipitation (Tang et al., 2018; Wehbe et al., 2017). With the development of meteorological satellites, remote sensing has become the main tool for estimating regional to global precipitation because of its wide spatial coverage and continuous observation periods. These series of satellites include the Global Precipitation Climatology Project (GPCP) (Huffman et al., 1997), the Tropical Rainfall Measuring Mission (TRMM) Multisatellite Precipitation Analysis (TMPA)(Huffman et al., 2007), the NOAA Climate Prediction Center (CPC) morphing technique (CMORPH) (Joyce et al., 2004), Precipitation Estimation from Remotely Sensed Information using Artificial Neural Networks (PERSIANN)(Sorooshian et al., 2000), Global Satellite Mapping of Precipitation (GSMaP) (Kubota et al., 2007), and Integrated Multisatellite Retrievals for Global Precipitation Measurement (GPM) (Hou et al., 2014). Although each product has its own more strengths in the capture of precipitation spatial patterns, there is a common issue, induced by its coarse spatial resolution (e.g., 0.1°-0.5°), greatly blocking the application of these products in hydrological and meteorological research at the local scale (Lin and Wang, 2011; Prakash et al., 2016; Chen et al., 2018).

To enhance the applications of current coarse-resolution precipitation products, a procedure that involves spatially downscaling these products to a high-resolution level has become an important solution. In recent decades, many downscaling methods have been proposed with the use of different satellite precipitation products. There are two major categories of downscaling methods: statistical downscaling and dynamical downscaling (Tang et al., 2016; Maraun et al., 2010). Statistical downscaling methods are mainly conducted by building the explanatory ability of the precipitation spatial distribution with fine-scale predictors, including topographic, geographic, and atmospheric variables, with the use of traditional regression methods (Xu et al., 2015; Mei et al., 2020), optimal interpolation techniques (Chao et al., 2018; Shen et al., 2014), multidata fusion (Rozante et al., 2020; Ma et al., 2021) or machine learning algorithms (He et

56   al., 2016; Baez-Villanueva et al., 2020). Comparatively, dynamical downscaling refers to the use of regional climate

57   models driven by global climate model output or reanalysis data to generate regional precipitation information (Rockel,

58   2015), which requires information related to complex physical processes of precipitation, such as atmospheric, oceanic

59   and surface information (Tang et al., 2016). Hence, spatial downscaling is achieved by modelling the conditional

60   distribution of precipitation at a fine scale to characterize the spatial structure of precipitation (Munsi et al., 2021;

61   Haylock et al., 2006).

62   Among the existing methods, due to the computational efficiency and the consideration of orography in

63   precipitation distribution, the statistical downscaling methods have been widely used in recent years. Most of them were

64   conducted with the use of predictors, such as topographic and vegetation factors (Immerzeel et al., 2009; Jia et al., 2011;

65   Jing et al., 2016a; Zeng et al., 2021). However, these predictors do not have physical connections with precipitation, they

66   act as important environmental variables influencing precipitation distribution. Consequently, the lack of the physical

67   background of this type method may introduce high uncertainty to the final downscaled results. Comparatively, surface

68   soil moisture (SSM) presents an obvious and strong physical connection with precipitation via their coupling and

69   feedback processes (Seneviratne et al., 2010). As indicated by Brocca et al. (2014), precipitation is the main driver of

70   SSM temporal variability. A sudden increase may occur in SSM after a rainfall pulse, followed by a smooth recession

71   limb driven by evapotranspiration and drainage. This relationship can be well reflected by an example of the time series

72   of precipitation and SSM from Dec 26 to 28, 2017 at station BRAGANCA, Portugal (Figure 1). A rapid increase in SSM

73   occurs after these rainfall events. Then, the moisture condition gradually becomes drier when there is no further rainfall.
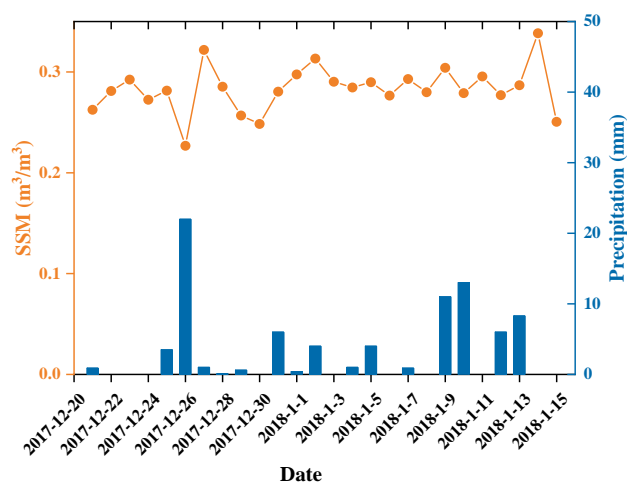
74

75   **Figure 1. Time series of observed precipitation and satellite observed SSM at station BRAGANCA, Portugal.**

76   According to this feature, SSM shows a big advantage in estimating precipitation and this connection was approved

77   by the SM2RAIN method proposed by Brocca et al. (2013). The Soil Moisture Analysis Rainfall Tool (SMART)

78   proposed by Chen et al. (2012) also improved the sub-monthly scale accuracy of a multidecadal global daily rainfall

79   product with a lower root mean square error (-13%) and a higher probability of detection (+5%). Recent applications of

80   this bottom-up approach further demonstrate the success of using SSM in precipitation estimation at coarse-resolution

81   scales (Wehbe et al., 2020; Brocca et al., 2016; Ciabatta et al., 2017; Brocca et al., 2019; Ciabatta et al., 2018). Thus, it

82   should be a very promising solution to improve the downscaling accuracy by introducing SSM in current downscaling

83   schemes. However, the availability of high-resolution SSM data is very limited and most of the current SSM products

84   have a spatial resolution of more than 10 km (Peng et al., 2021), placing significant restrictions on these applications.

85   Furthermore, suffering from an indirect physical connection between topographic and vegetation factors and

86   precipitation, a large amount of downscaling research has been conducted at monthly or annual scales, and the lack of

87   daily high-resolution precipitation data mismatches the requirements of regional hydrological modelling and applications.

88   In recent decades, there has been substantial progresses in soil moisture downscaling studies (Long et al., 2019;

89   Sabaghy et al., 2020; Wen et al., 2020; Merlin et al., 2008; Piles et al., 2014; Peng et al., 2016; Tagesson et al., 2018;

90   Zhao et al., 2021), which makes the availability of high-resolution soil moisture data possible at a daily scale. Thus, the

91   main objective of this study is to establish a soil moisture-based precipitation downscaling (SMPD) scheme as a novel

92   way of obtaining fine-scale precipitation by fragmenting the coarse-pixel rainfall to fine-scale pixels. For this purpose,

93   the 25-km European Space Agency (ESA) Climate Change Initiative (CCI) SSM product is used to derive 1-km SSM

94   data based on the seamless downscaling method proposed by Zhao et al. (2021). Based on the inversion of the water

95   balance equation, a simplified model for estimating precipitation is constructed with the use of the downscaled 1-km

96   seamless soil moisture data and the vegetation index derived from the Moderate Resolution Imaging Spectroradiometer

97   (MODIS) observation and then applied to daily GPM precipitation to obtain the daily downscaled precipitation estimates.
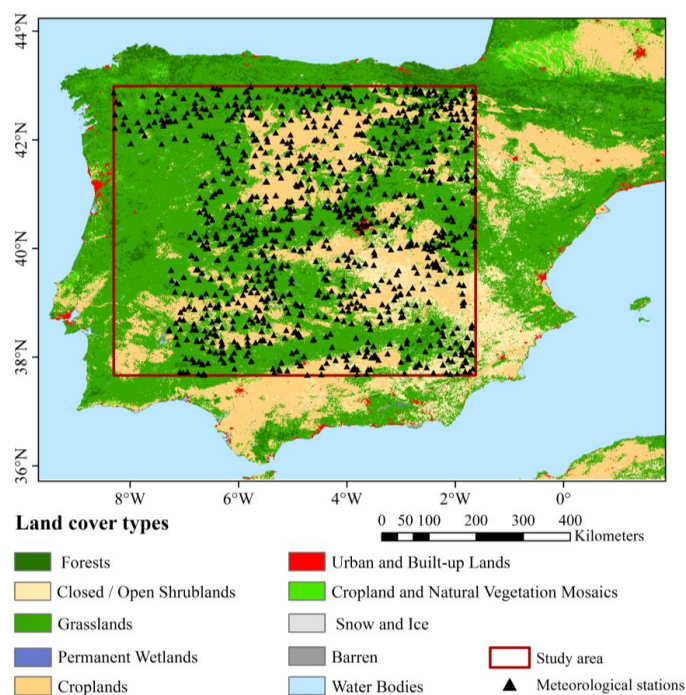
98   **2 Study area and datasets**

99   **2.1 Study area**

100   The central part of the Iberian Peninsula was selected as the study area (Figure 2). It is located in the southwestern

101   Europe between 37.66°–42.99°N and 8.30° W–1.63° E. The region has a distinctly seasonal mild climate, with hot and

102   dry summers inland, cooler summers along the coast, and cold and wet winters. Precipitation presents a double peak

103   pattern, typical from the Mediterranean, with increased precipitation in Autumn and Spring. The central part of the study

104   area has a temperate continental climate, while the southern part has a Mediterranean climate, with warm and humid

105   winters and hot and dry summers. Generally, the south is dry and warm, while the north is relatively wet and cool.

106   Enhanced by the complex topographic pattern and diverse land cover conditions, this region has a highly heterogeneous

107   spatial environment, which makes this region a satisfactory candidate for precipitation downscaling. In addition, there

108   are many meteorological stations with long-term precipitation measurements in this area, which is an important

109   prerequisite for this study.

110

111   **Figure 2. Geolocation and land cover map of the study area. The black triangles denote the meteorological stations collected in this**
112   **study.**

113   **2.2 Datasets**

114   **2.2.1 GPM IMERG satellite precipitation data**

115   As the successor of the successful Tropical Rainfall Measuring Mission (TRMM), the Global Precipitation

116   Measurement (GPM) not only expands the measurement range and temporal and spatial resolution of the TRMM, but

117   also estimates the instantaneous precipitation more accurately, especially light-intensity precipitation (i.e., <0.5 mm h^{-1})

118   and falling snow (Hou et al., 2014; Huffman et al., 2015), GPM-IMERG (Integrated Multisatellite Retrievals for GPM)

119   is the level 3 multisatellite precipitation algorithm of the GPM, which combines precipitation information measured from

120   the microwave sensor and infrared sensors onboard GPM constellations and monthly gauge precipitation data, and

121   IMERG employs the 2014 version of the Goddard Profiling Algorithm (GPROF2014) to compute precipitation estimates

122   from all passive microwave (PMW) sensors onboard GPM satellites, which is a significant improvement compared with

123   TMPA (GPROF2010) (Huffman et al., 2015; Huffman et al., 2020). Hence, it has attracted much attention in the satellite

124   remote sensing of precipitation.

125   Currently, the GPM product provides near-real-time products (early and late run) and postural-rime products (final

126   run) from sub-hourly to monthly resolution at a $0.1°×0.1°$ spatial scale. Owing to the infusion of multiple data, such as

127   microwave, infrared, radar, and Global Precipitation Climatology Centre (GPCC) rain gauge data (Hou et al., 2014), the

128   GPM-IMERG final run product provides more accurate estimates over the globe with a relatively long time series (June

129   2000- present) with a minimum latency of 3.5 months. In this study, the GPM-IMERG final run daily precipitation

130   product (downloaded from https://pmm.nasa.gov/data-access/downloads/gpm) was adopted as the downscaling object.

131   A three-year period from 2016 to 2018 was selected to verify the performance of the downscaling method based on the

132   availability of rain gauge data.

2.2.2 ESA CCI surface soil moisture data

134   The Soil Moisture CCI project is a part of ESA's Program on the Global Monitoring of Essential Climate Variables

135   (ECV), which was initiated in 2010 and has produced an updated SSM product annually since 1978 (Colliander et al.,

136   2017). The ESA CCI SSM series contains three separate SSM datasets, which are derived from active and passive

137   microwave remote missions as well as a combination of both, and the combined ESA CCI SSM product (version 04.7)

138   provides a spatial resolution of 0.25° and a temporal resolution of one day on a global scale (http://www.esa-

139   soilmoisture-cci.org/).

140   The combined ESA CCI SSM product provides the amount of water in the surface soil (approximately the top 5

141   cm), which integrates observations derived from 11 microwave sensors including active sensors such as Advanced

142   Scatterometer-A/B (ASCAT-A/B) and European Remote-sensing Satellite-1/2 (ERS-1/2), and passive sensors such as

143   Special Sensor Microwave Imager (SSM/I), the Scanning Multichannel Microwave Radiometer (SMMR), the TRMM

144   Microwave Imager (TMI), AMSR-E, WindSAT, AMSR2 and SMOS (Gruber et al., 2019). Previous evaluation studies

145   have demonstrated that ESA CCI SM generally agrees well with the spatial and temporal patterns estimated by land

146   surface models and in situ observations (Dorigo et al., 2017; Mcnally et al., 2016). Therefore, this combined product

147   was used in this study for the study period of January 1, 2016 to December 31, 2018 to obtain fine-resolution soil

148   moisture to assist in precipitation downscaling.

149   **2.2.3 Normalized difference vegetation index (NDVI)**

150   NDVI is an important indicator of vegetation activity (Pan et al., 2021; Zhang et al., 2020a; Neinavaz et al., 2020),

151   especially for surface evapotranspiration (Joiner et al., 2018; Maselli et al., 2020). Therefore, it also presents a positive

152   correlation with precipitation (Quiroz et al., 2011; Birtwistle et al., 2016). The intuitive correlation between rainfall and

153   plant biomass represented by NDVI would enhance the downscaling study with high-resolution NDVI data. In this study,

154   the   NDVI   data   were   obtained   from   the   MODIS/Terra   16-day   vegetation   index   product

155   (https://lpdaac.usgs.gov/products/mod13a2v006/). It is a 16-day composite product obtained by choosing the best

156   available pixel value from all the acquisitions over 16 days with the spatial resolution of 1 km.

157   **2.2.4 Rain gauge data**

158   Daily precipitation data collected from 1027 rain gauge stations from 2016 to 2018 with different land cover

159   properties were used as the independent validation of the downscaled results in this study. These data were provided by

160   the Spanish State Meteorological Agency (AEMET). The distribution of the selected stations is mapped in Figure 2.

161   **3 Methodology**

162   **3.1 Soil moisture-based precipitation estimation model**

163   The soil water balance equation for a layer depth Z can be described by the following expression:

164
$$Z\frac{ds(t)}{dt} = p(t) - g(t) - e(t) - r(t)$$
(1)

165   where $s(t)$ [-] is the relative saturation of the soil or relative SSM, t is the time and $p(t)$, $r(t)$, $e(t)$ and $g(t)$ are the

166   precipitation, runoff, evapotranspiration, and drainage rate, respectively. By rearranging Eq. (1), precipitation can be

167   depicted as a function of SSM, runoff, evapotranspiration, and drainage rate. Based on this rule, Brocca et al. (2013)

168   proposed a bottom-up approach (SM2RAIN) by doing "hydrology backward" to infer precipitation with the use of

169   variations in SSM sensed by microwave satellite sensors. To perform this estimation, the model is simplified in different

170   ways by neglecting different components in Eq. (1) (Brocca et al., 2014; Massari et al., 2014) and the comparison study

171   indicated that the average contribution of surface runoff and evapotranspiration components amounts to less than 4% of

172   the total rainfall, while the soil moisture variation (63%) and subsurface drainage (30%) terms provide a much greater

173   contribution (Brocca et al., 2015). Although the contribution of evapotranspiration is relatively small, the dry

174   Mediterranean climate in most of this region emphasizes its importance. Therefore, the precipitation estimation model

175   was reorganized by only neglecting the runoff component:

176
$$p(t) = Z\frac{ds(t)}{dt} + g(t) + e(t)$$
(2)

177   In Eq. (2), the drainage rate is approximated by considering the relation in Famiglietti and Wood (1994) to include

178 the contribution of both deep percolation and subsurface runoff (interflow plus baseflow):

179
$$g(t) = as(t)^b$$
(3)

180 where a and b are two parameters expressing the nonlinearity between drainage rate and soil saturation. Regarding the

181 evapotranspiration component, there are many methods have been developed to estimate ET in natural ecosystems

182 (Sheffield et al., 2009; Mu et al., 2009; Carpintero et al., 2020). For instance, the daily evapotranspiration can be derived

183 as a function of the vegetation index (VI) and air temperature (T_a) (Nagler et al., 2005a; Nagler et al., 2005b):

184
$$e(t) = a\left(1 - e^{-bVI}\right)\left(c\big/\left(1 + e^{-(T_a - d)/e}\right) + f\right)$$
(4)

185 where the coefficients (a-f) were determined by conducting regression between ET and the independent variables.

186 Although there is the air temperature in Eq. (4) to specify the impact of the air temperature difference within a wide

187 range, this term can be assumed to be invariant when considering the pixels to a small extent. Therefore, Eq. (4) can be

188 further simplified with the use of the NDVI as follows:

189
$$e(t) = c\left(1 - e^{-kNDVI}\right)$$
(5)

190   Based on the above approximation, the soil moisture-based precipitation estimation model was finally expressed

191 by the following equation:

192
$$p(t) = Z\frac{ds(t)}{dt} + as(t)^b + c\left(1 - e^{-kNDVI}\right)$$
(6)

193 where d$s(t)$/dt can be calculated as the difference between the SSM estimates on nearby days. According to the

194 simplification in Eq. (5), this proposed model is appropriate for estimation to a local extent.

3.2 SMPD method

196   To perform precipitation downscaling, an important prerequisite is the assumption of spatial invariancy in the

197 precipitation estimation model described in Eq. (6) at coarse and fine scales, which is also the basis of many related

198 downscaling studies aiming at other parameters, such as soil moisture and temperature (Zhao et al., 2018; Mishra et al.,

199 2018; Hutengs and Vohland, 2016; Ebrahimy and Azadbakht, 2019). Therefore, the estimation model established at the

200 10-km level is thought to be applicable at the 1-km level. Additionally, to preserve the mean rain rate over each coarse-

201 scale pixel, the bias should be corrected by redistributing the residual to each fine-scale pixel. According to the above

202 principle, the downscaling method consists of the following parts.

3.2.1 Generation of daily SSM at a fine resolution

As shown in Eq. (6), SSM is an important variable in the estimation model. The ESA CCI SSM product can only

provide coarse-resolution SSM data with unexpected gaps. To obtain daily SSM at a 1-km resolution, the seamless SSM

downscaling method proposed by Zhao et al. (2021) is a good choice to achieve this goal. This downscaling method

mainly includes three steps: 1) filling gaps in the 25-km ESA CCI SSM maps with neighbourhood information based on

a local linear regression method, 2) estimating the 1-km regression SSM and coarse-resolution residual with a

geographically weighted regression (GWR) method, and 3) downscaling the coarse-resolution residual to 1-km spatial

resolution with the area-to-point kriging (ATPK) method and obtaining the fine-resolution SSM. For details about the

downscaling method, please refer to Zhao et al. (2021).

3.2.2 Calibration of the precipitation estimation model with an adaptive window method

Before model calibration, the 1-km downscaled SSM data and the NDVI data were first aggregated into a 10-km

scale to spatially match the spatial resolution of the GPM-IMERG product. Then, these data were applied to calibrate

the coefficients of the precipitation estimation model. As introduced in section 3.1, the application of this model requires

a prerequisite to work at a local extent because of the simplification of the evapotranspiration estimation. Therefore, a

local window with a radius from 3 to 7 cells was adopted in the fitting process. Initialized from the size of 3 cells, the

optimal window size was adaptively selected when the correlation coefficient (CC) of the fitting result reached to the

maximum value. This adaptive method was applied to each coarse-resolution pixel with a sliding window, and the model

coefficients of this pixel were derived. During the model calibration, coarse pixels with zero precipitation were excluded.

$$p_{10km}(t) = Z\left(SSM_{10km}(t) - SSM_{10km}(t-1)\right) + aSSM_{10km}(t)^b + c\left(1 - e^{-kNDVI_{10km}}\right) \tag{7}$$

3.2.3 Residual correction and fine-scale precipitation estimation

Based on the calibrated estimation model coefficients in Eq. 7, the precipitation estimates determined with this

model can be calculated for each high-resolution pixel within the corresponding coarse pixel:

$$p_{1km}^{m}(t) = Z\left(SSM_{1km}(t) - SSM_{1km}(t-1)\right) + aSSM_{1km}(t)^b + c\left(1 - e^{-kNDVI_{1km}}\right) \tag{8}$$

However, there is a residual between the original precipitation value of each coarse-resolution cell pixel p_{10km}^{o} and

the mean value of the estimated precipitation of all fine-resolution pixels within this cell. For the n 1-km pixels within

each coarse-resolution cell, the residual is expressed as follows:

229
$$R_{10km} = p^o{}_{10km} - \sum_{i=1}^{n} p^m_{1km,i} \tag{9}$$

230   To meet the requirement of value preservation in the downscaling process, the residual should be corrected by

231   redistributing it to each fine-resolution pixel. The kriging interpolation method was used here to obtain the interpolated

232   residuals at fine-scale pixels. The high-resolution residual was expressed as a weighted integration of the residuals of

233   the neighbouring coarse-resolution cells.

234
$$R_{1km,ij} = \sum_{k=1}^{n} \lambda_k R_{10km,k} \tag{10}$$

235   where $R_{1km,ij}$ represents the estimated precipitation of the ith high-resolution residual pixel in the coarse-resolution cell j,

236    $R_{10km,k}$ represents the kth coarse-resolution cell in the self-adaptive window, n is the number of cells in the self-adaptive

237   window, and λ_k is the weight coefficient derived from the kriging interpolation.

238   Finally, the high-resolution precipitation was obtained by integrating the fine-resolution estimates via Eq. (8) and

239   the residual term in Eq. (10):

240
$$p_{1km} = p^m_{1km} + R_{1km} \tag{11}$$

241   **3.3 Validation**

242   To better assess the performance of the proposed downscaling method, the downscaled GPM results were validated

243   by observations from the collected stations in the study area at both daily and monthly scales. The evaluation metrics

244   include the correlation coefficient (CC), root mean square error (RMSE), and the relative bias (BIAS). They are defined

245   as follows:

246
$$CC = \frac{\sum_{i=1}^{n} (S_i - \bar{S})(P_i - \bar{P})}{\sqrt{\sum_{i=1}^{n} (S_i - \bar{S})^2 (P_i - \bar{P})^2}} \tag{12}$$

247
$$RMSE = \sqrt{\frac{\sum_{i=1}^{n} (S_i - P_i)^2}{n}} \tag{13}$$

248
$$BIAS = \frac{\sum_{i=1}^{n} (S_i - P_i)}{\sum_{i=1}^{n} P_i} \tag{14}$$

249   where P_i and S_i are the precipitation measured by the rain gauge and downscaled satellite precipitation at station i, respectively.

250    $\bar{P}$ is the mean value of all rain gauge observations, and $\bar{S}$ represents the mean value of the downscaled satellite precipitation

251   at all the stations, and n is the number of stations in this analysis.

252   Additionally, two metrics reflecting the capability of capturing precipitation events were introduced in the

253   assessment: the false alarm ratio (FAR) and critical success index (CSI). The FAR refers to the proportion of the

254   precipitation events that the satellite falsely detects and the rain gauges do not recognize it. The CSI represents the

255   fraction of precipitation events correctly detected by satellites to the total number of observed or detected rainfall events.

256   The definition of a rainfall accumulation "event" is one-day rainfall accumulation in excess of a given threshold of 0.1

257   mm. These two terms are depicted as below:

258     $$FAR = \frac{F}{H + F} \tag{15}$$

259     $$CSI = \frac{H}{H + F + M} \tag{16}$$

260   where H indicates the precipitation events concurrently detected by rain gauges and satellites, M indicates the

261   precipitation events detected by rain gauges but not detected by satellites, and F indicates the precipitation events

262   detected by satellites but not detected by rain gauges.

263   **4 Results**

264   **4.1 Accuracy of the soil moisture-based precipitation estimation model**

265   Before the downscaling process, the performance of the soil moisture-based precipitation estimation model was

266   evaluated first. Figure 3 shows the maps of the mean value of the daily CCs and RMSEs during the period of 2016–2018

267   and their standard deviation (STD) by comparing the precipitation estimated with the proposed estimation model and

268   the original GPM precipitation product. Most of the CC values are above 0.7 with an average value of 0.71, and most of

269   the RMSE values are within the range from 0.50 to 1.00 mm, with an average value of 1.00 mm. This result indicates

270   the good consistency and small error between the estimated precipitation and the original product. Furthermore, in view

271   of the STD map, it represents the variability in CC and RMSE during the period. The CC-STD values are within the

272   range from 0.18 to 0.28 with an average value of 0.23, most of the RMSE-STD values are concentrated in the range of

273   0.5 to 1.5 mm, and only a few are in the range of more than 3 mm, with an overall mean of 1.39 mm. Combined with

274   the frequency distributions of CC and CC-STD, RMSE, and RMSE-STD, the proposed estimation model can generally

275   capture the precipitation with soil moisture variations and it has a relatively stable performance over three years.
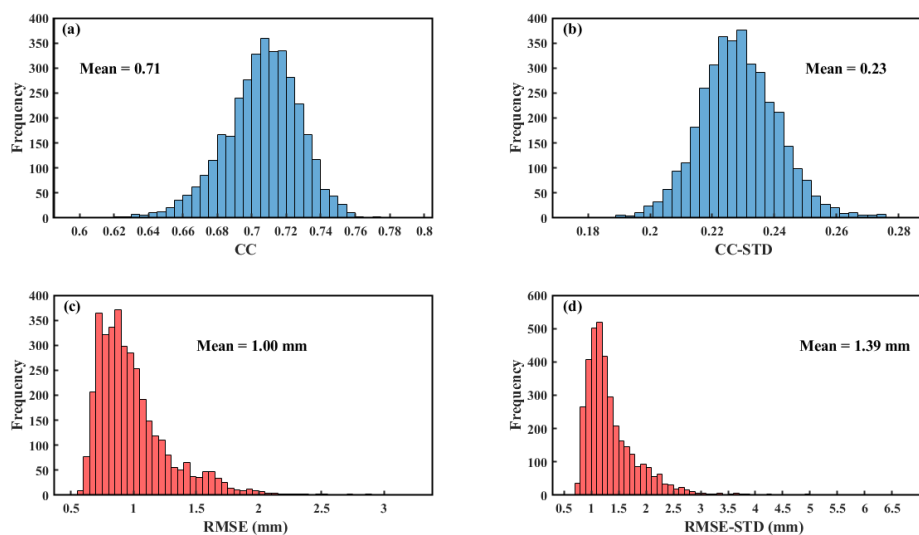
Figure 3. (a) Maps of the mean value of the correlation coefficient (CC), (b) mean standard deviation of the CC (CC-STD), (c) mean root mean square error(RMSE), and (d) mean standard deviation of the RMSE (RMSE-STD) between the precipitation estimated with the soil moisture-based estimation model and the original GPM product during the period of 2016-2018. The mean value represents the average value of the corresponding index in the whole study area.

According to the fitting performance assessment with the original GPM product, the soil moisture-based precipitation estimation model has been approved to be able to capture the variation of precipitation with acceptable accuracy. Therefore, the fitted estimation model at 10 km scale was applied to the SSM and NDVI data at 1 km scale to obtain the estimated high-resolution precipitation. Then, the residual between the estimated precipitation and the original precipitation was calculated. The kriging interpolation method was implemented to redistribute the residuals to the estimated values at 1 km scale. Finally, the downscaled daily GPM precipitation products were obtained with the integration of the estimated precipitation and the interpolated residual. The performance of the downscaled results was further evaluated by spatio-temporal distribution and observations from meteorological stations.

**4.2 Overall performance of the downscaled precipitation**

4.2.1 Spatial distribution

To demonstrate the advantages of the downscaling results, two separate days (Jul. 7 and Nov. 25, 2017) in the dry season and wet season were selected to compare the original coarse-resolution precipitation data and the downscaled high-resolution precipitation data (Figure 4). From the visual inspection, the spatial distributions of the downscaled

294   precipitation are highly consistent with those of the original ones in both seasons, especially for the distribution of the

295   precipitation centers (>50 mm/day). The downscaled results maintained the original precipitation pattern in the GPM

296   product, which can be reflected well by the very similar histograms of the original and downscaled precipitation on these

297   two days, as shown in Figure 4c and f. In addition to their consistency, the downscaled results present higher spatial

298   heterogeneity than the coarse-resolution product, which provides much more detailed information on the precipitation

299   distribution within each coarse-resolution cell. More importantly, the downscaled results prevent the blockiness at the

300   edges of the coarse-scale pixels.
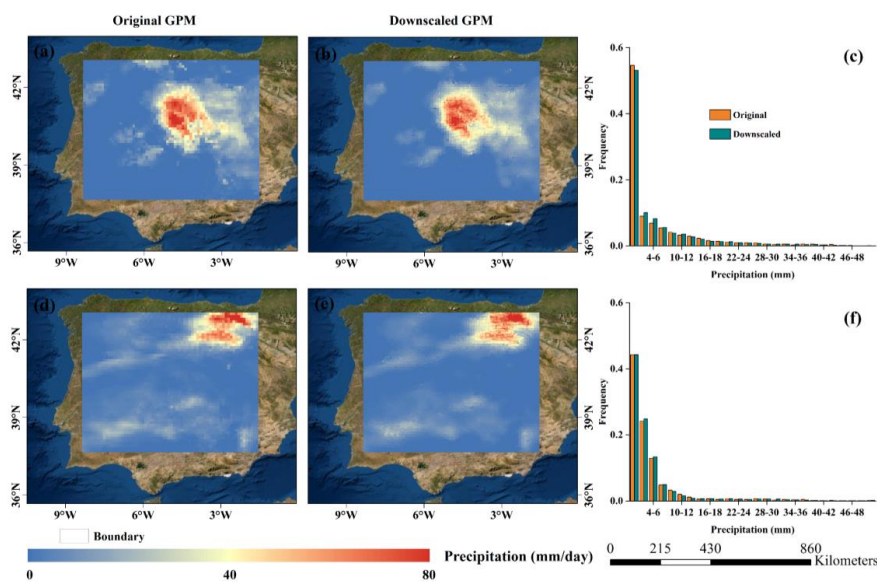
301

302   **Figure 4. Original daily GPM precipitation products, downscaled results, and their frequency histograms on July 7, 2017(a-c) and**

303   **November 25, 2017(d-f).**

304

305   **4.2.2 Temporal variability**

306   In addition to the spatial distribution analysis, the temporal variation in the downscaled precipitation was further

307   evaluated by introducing the downscaled results from Dec. 8 to Dec. 11, 2017. Figure 5 shows the daily maps of the

308   original precipitation and downscaled precipitation. For the spatial distribution, both the original GPM precipitation

309   product and the downscaled result have almost the same patterns on different days. Not only heavy rainfalls but also

310   light rainfalls can also be captured by the proposed downscaling method in most circumstances. Moreover, the temporal

311   variability in the daily precipitation was also preserved after the downscaling, and some outliers in the coarse-resolution

312   GPM product were effectively filled with valid values, as shown by the downscaling results on Dec. 11 in Figure 5.
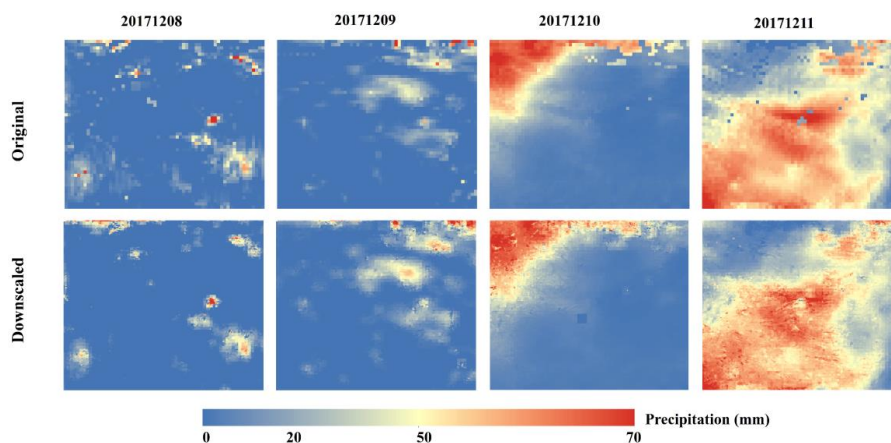
313
314   **Figure 5. Original daily GPM precipitation product and corresponding downscaled results from Dec.8th to Dec.11th, 2017.**

315   **4.3 Validation with rain gauge measurements**

316   **4.3.1 Validation at the daily scale**

317   To quantitatively evaluate the performances of the downscaling results, the daily original-scale GPM precipitation

318   data and the downscaled results are compared separately with the precipitation measurements from the selected 1027

319   meteorological stations. Two metrics, rainfall events and precipitation volumes, were used to evaluate the performances

320   of both datasets. As shown by the density plots in Figure 6a, there is a relatively high uncertainty in the original GPM

321   precipitation product compared with the in-situ observation with a CC of 0.60, an RMSE of 4.99 mm and a BIAS of 9%.

322   The GPM product generally has an overestimating effect at daily scale. These differences may be attributed to the

323   differences in the spatial representativeness of both observations (one for the average value over a grid cell and one for

324   a single point). Because of the value preservation during the downscaling process, the downscaled result also has a

325   validation effect similar to that of the GPM product (Figure 6b). However, compared with the original GPM product,

326   the downscaled result shows an overall improvement in terms of CC, RMSE, and BIAS. There is a slight increase in CC,

327   with its value increasing from 0.60 to 0.61. In contrast, both the RMSE and BIAS have a moderate reduction, with

328   decreases of 0.16 mm and 4%, respectively. For rainfall event assessment, the downscaled result remarkably enhanced

329   the ability to identify rainfall events at every station when compared with the original GPM product. Both the FAR and

330   CSI were moderately enhanced relative to those of the original GPM data, with a decrease in the FAR from 0.52 to 0.47

331   and an increasing CSI from 0.44 to 0.48. The comparison showed that the downscaled results could better detect

332   precipitation occurrence than the original GPM product. The increase in spatial heterogeneity in the downscaled result

333   assists rainfall event detection.

334
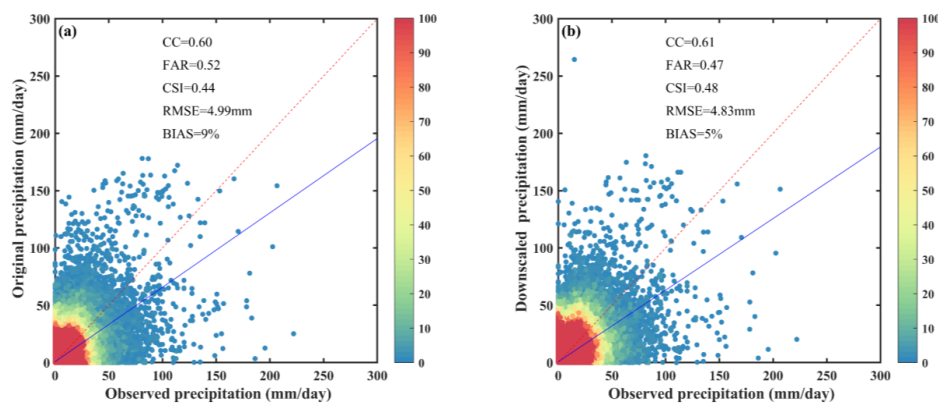
Figure 6. Density plots of the original GPM precipitation product (a) and the downscaled results (b) plotted against daily precipitation recorded by available meteorological stations over the study period. The red dotted line represents the 1:1 line and the blue solid line represents the fitting line.

338   In addition to the validation over the whole period, further investigation was performed for the downscaled results

339   at individual months. Table 1 lists the evaluation indicators of the downscaled and original precipitation against rain

340   gauge observations from 1027 stations. In general, the downscaled results show similar accuracy performance among

341   different months from the detection accuracy of precipitation events reflected by FAR and CSI. However, from the

342   RMSE values, seasonal differences can be detected. The dry season months from June to September have relatively

343   smaller RMSE values than other months. It is not because of the better performance of the proposed method in these

344   months but the inherent small precipitation of these months enables the low value of RMSE. This feature can be also

345   detected from the evaluation of the original data. About the downscaled results performance, the downscaled data have

346   better accuracy in detecting precipitation events according to the improvement in FAR and CSI in each month.

347   Comparatively, the correlation feature of the downscaled results shows a small improvement than the original data,

348   represented by the CC values every month. Meanwhile, there are all decreasing trends in terms of RMSE and the

349   improvements in the wet seasons from October to May are relatively bigger than the dry season months. For the BIAS

350   values, the improvements are also very clear with the extent from 3% to 7%. The monthly comparison further indicated

351   the improvement from the downscaled results which not only maintain the temporal correlation characteristics of the

352   original data with the rain gauge station observations but also improve the absolute accuracy according to the refinement

353   of CSI, FAR, RMSE, and BIAS via introducing more detailed information in the downscaling scheme.

354 **Table 1.** Validation of the downscaled precipitation data, original GPM precipitation data with the daily precipitation measured by the

355 selected stations at each month.

	Original					Downscaled				
	CC	FAR	CSI	RMSE (mm)	BIAS	CC	FAR	CSI	RMSE (mm)	BIAS
January	0.57	0.49	0.47	6.36	14%	0.58	0.43	0.48	6.14	10%
February	0.56	0.49	0.47	6.83	7%	0.57	0.42	0.50	6.51	2%
March	0.66	0.45	0.52	6.27	-3%	0.66	0.40	0.54	6.10	-6%
April	0.60	0.45	0.51	5.67	9%	0.60	0.41	0.53	5.44	5%
May	0.60	0.46	0.50	4.78	5%	0.61	0.42	0.53	4.59	1%
June	0.55	0.48	0.49	3.31	15%	0.56	0.43	0.52	3.18	11%
July	0.63	0.49	0.48	2.72	24%	0.63	0.44	0.52	2.64	19%
August	0.61	0.50	0.48	2.05	14%	0.60	0.44	0.51	2.04	9%
September	0.50	0.51	0.47	2.74	34%	0.50	0.45	0.50	2.69	27%
October	0.57	0.51	0.46	4.34	12%	0.58	0.45	0.50	4.22	8%
November	0.59	0.50	0.47	6.18	10%	0.60	0.45	0.50	5.99	6%
December	0.59	0.51	0.46	5.66	14%	0.58	0.45	0.50	5.57	11%

356 **4.3.2 Spatial distribution of the daily validation at all stations**

357 In addition to the general evaluation with the measurements from all stations, the downscaled results are separately

358 validated by the observations from each station, and the results are illustrated in Figure 7. In general, the downscaled

359 precipitation estimates produce less error than the original GPM precipitation with respect to all overall error statistics

360 from 2016 to 2018, with an increase of CC values from 0.62 to 0.63, a decrease of RMSE values from 4.80 mm to 4.63

361 mm, a decrease of BIAS values from 17% to 13%, a decrease of FAR values from 0.50 to 0.45, an increase of CSI values

362 from 0.47 to 0.50, respectively, which show moderate improvement compared to that of the original GPM products.

363 Moreover, from the frequency histogram of validation indicators at 1027 stations, the downscaled results present a better

364 correlation with rain gauge observations with most of the CC values being above 0.71 in the central and north-western

365 regions. Regarding RMSE in Figure 7e, the validation at 728 stations derives a low RMSE value (lower than 5.01 mm)

366 and these stations are mainly located in the central and south-eastern regions. In comparison, the validation with high

367 RMSE is majorly occurred in the north-western regions due to the originally bigger annual mean precipitation. Figure

368 7f clearly shows the improvement of the downscaled result with regard to RMSE. For BIAS, there is a relatively wide

369 range from -72% to 99% in the whole region, systematic overestimation is observed at 685 stations, and underestimation

370 is also observed at 342 stations. After downscaling, the overestimation was lightened. About the rainfall event assessment,

371 most of the CSI values are higher than 0.48 at these stations and the FAR values are generally lower than 0.46, as shown

372   in Figure 7 j-o. It can also be seen that the detection accuracy of precipitation events in the humid northern region is

373   better than that in the southern region with less precipitation. Those results indicate that the fitting relationship between

374   observed precipitation and downscaled GPM is good in the northwest region, but the errors in precipitation volumes are

375   large in north-western regions due to rich precipitation. In addition, because the improvement in rainfall events

376   introduced by the downscaling method is not limited to specific locations and covers the whole area, the downscaled

377   results are more accurate in describing spatial precipitation details.
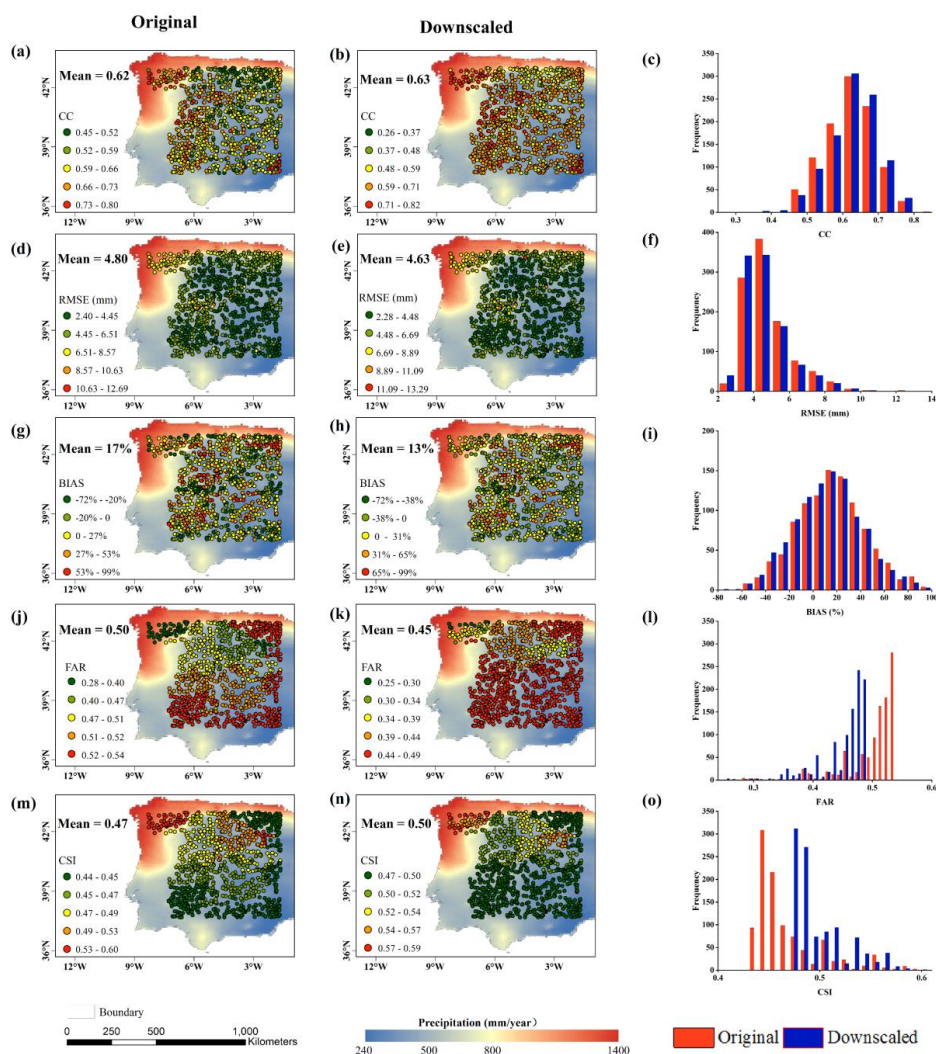

378

379   **Figure 7. CC (a-c), RMSE (d-f), BIAS (g-i), FAR (j-l), CSI (m-o) and corresponding frequency distributions for daily precipitation**

380   **of original and downscaled GPM precipitation estimates at 1027 gauge sites during 2016–2018. The background value represents**

381   **the original GPM annual average precipitation value from 2016 to 2018**

382   Generally, the improvement from the overall performance for the downscaled results in Figure 7 is attributed to the

383   number of improvements in the validation site indicators that occur between the original GPM product, the downscaled

384   results, and the observation stations at the daily scale. The downscaled results outperformed the original product in the

385   detection accuracy of rainfall events and precipitation volumes, and the numbers of improvements in CSI and FAR are

386   1008 and 1026, respectively. Similarly, the number of improvements of CC, RMSE, and BIAS are 765, 886, and 884,

387   respectively. The downscaled results are more accurate than the original product when they are validated by field

388   measurements at most stations. In summary, the improvement in the precipitation downscaled by the SMPD method

389   occurs at most rain gauge stations. The evaluation demonstrates the ability of this method to increase spatial

390   heterogeneity to enhance the correlation with field measurements while also retaining the original GPM spatial

391   distribution pattern. All the above results clearly prove the effectiveness of the downscaling method, which enhances

392   daily GPM precipitation in both spatial information and accuracy.

393   **4.3.3 Validation at the monthly scale**

394   In addition to the validation at the daily scale, the downscaling results were further evaluated at the monthly scale

395   by integrating the daily results into the monthly amount. Figure 8 shows the multiannual average maps of the monthly

396   precipitation from 2016 to 2018, including the original GPM product and the downscaled results. Similar to the daily

397   comparison, the monthly distributions of both datasets have quite similar patterns over different months. The northern

398   part of the study area has more precipitation than the southern part. The downscaled results maintain the precipitation

399   centers in each month and depict the distributions around the centers well. The downscaled results can provide more

400   detailed information regarding the spatial distribution.
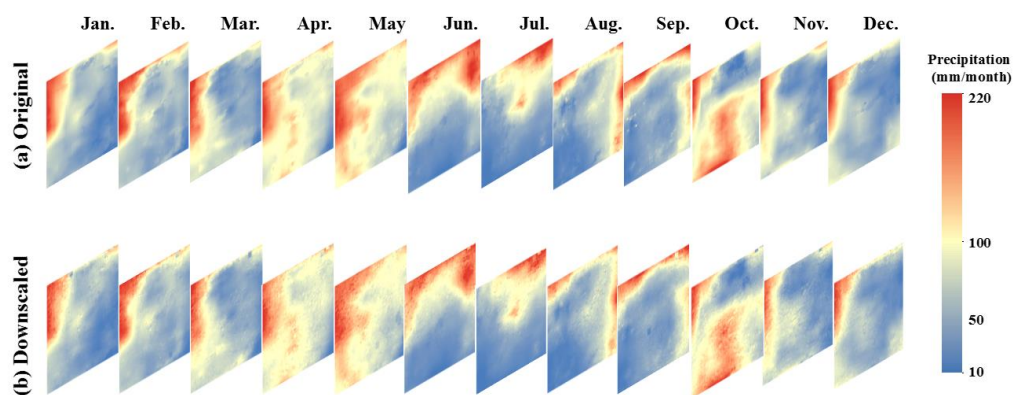
401

402   **Figure 8. Spatial distribution of the multiannual mean value of monthly precipitation for the original GPM product (first line) and**
403   **the downscaled results (second line) from 2016 to 2018.**

404   By collecting the monthly precipitation of each station, the accuracy of the monthly precipitation from the original

405   and downscaled data was further quantitatively assessed. As shown in Figure 9a, after temporal integration, the

406   uncertainty in the daily observation was greatly reduced in the monthly precipitation of the original GPM product. There

407   is a significant increase in CC from 0.60 in Figure 6a to 0.83 in Figure 9a. However, systematic overestimation still

408   occurs. After spatial downscaling, although there is no big change in terms of CC, both the RMSE and BIAS are clearly

409   improved based on a comparison of the density plots in Figure 9a and b. For the analysis of the improvement ratio, only

410   the performances of CC, RMSE, and BIAS are analyzed because the FAR and CSI mainly reflect the rainfall events at

411   the daily scale. Among the 1027 stations, the numbers of stations with improvements during the validation in terms of

412   CC, RMSE, and BIAS are 734, 587, and 912, respectively. Combined with the overall validation and individual

413   validation, the downscaled results at the monthly scale outperformed the original GPM product. The evaluation shows

414   that the downscaling method also presents a good accuracy in the downscaling results and high robustness at the monthly

415   scale.
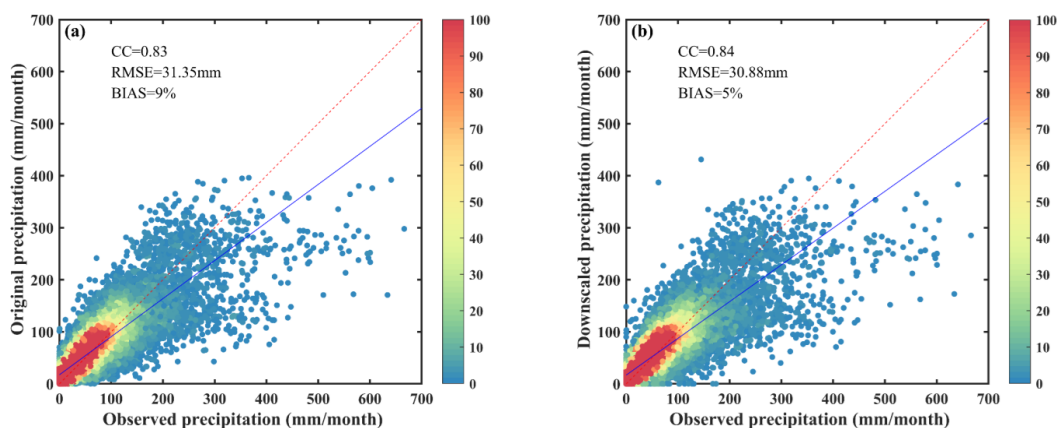
416

417   **Figure 9. Density plots of the original GPM precipitation product (a) and the downscaled precipitation data (b) plotted against the**

418   **monthly precipitation measured by the selected stations during the period from 2016 to 2018.**

419   **5 Discussion**

420   In this study, a spatial downscaling method for coarse-resolution precipitation products was proposed to produce

421   high-spatial resolution precipitation data at a 1 km scale with the use of 1-km SSM data downscaled from microwave

422   remote sensing estimations. To establish the connection between SSM and precipitation, a simplified precipitation

423   estimation model based on the surface water balance equation was developed with inspiration from the SM2RAIN model

424   proposed by Brocca et al. (2014). By calibrating the model coefficients with a self-adaptive window at the coarse-

425   resolution scale, the precipitation model was applied to high-resolution variables to obtain the high-resolution estimates.

426   Compared with previous downscaling methods that mainly establish empirical relationships with surface variables, such

427   as NDVI and topographic factors, this method introduces the physical relationship between SSM and precipitation via

428   the water balance equation and has a solid physical basis. Therefore, the validation analysis conducted at both daily and

429   monthly scales indicated that the downscaled precipitation data outperformed the original product in most circumstances

430   and presented high robustness over three years with different rainfall strengthens.

431   In general, the SMPD method adopted the bottom-up approach in precipitation estimation, in which the variations

432   in SSM sensed by microwave satellite sensors have a strong connection with rainfall amounts according to the principle

433   of water balance (Brocca et al., 2016; Mao et al., 2018; Brocca et al., 2014). After a sudden increase in soil moisture

434   induced by rainfall event, the moisture condition gradually becomes drier when there is no further rainfall. Therefore,

435   this method has a clear physical mechanism and is the only downscaling method using SSM as the key driving factor.

436   Comparatively, the traditional statistical downscaling methods were established based on the statistical relationship

437   between environmental factors and precipitation. Take the spatial interpolation method as an example, although the

438   application of this method is convenient, the accuracy of the interpolated precipitation data is limited by the rainfall

439   gauge density, especially in mountainous watershed with complex topography (Zhang et al., 2020b; Guo et al., 2021).

440   The high dependency of in-situ measurements constrains its applications in area with few observations. In contrast, the

441   SMPD method breaks the limitation caused by the rainfall gauge density and has a broader application prospect. To

442   further demonstrate the advantage of the SMPD method, it is beneficial to compare the validation accuracy of this method

443   with the validation accuracies of existing downscaled approaches, as shown in Table 2. In current existing downscaling

444   studies, the involvement of daily SSM ensures downscaling at a daily scale is rarely considered. However, the

445   relationship between SSM and precipitation ensures the daily downscaling in the proposed SMPD method.

446   Comparatively, although Yan et al. (2021) conducted daily precipitation downscaling with the use of the random forest

447   (RF) method, the RSME value was considerably lower than that of the SMPD method. Moreover, this machine learning

448   method is highly dependent on the available training dataset. Comparatively, the daily or sub-daily downscaling studies

449   conducted by Long et al. (2016) and Chao et al. (2018) have relatively better performances in terms of RMSE and CC,

450   respectively. However, the incorporation of gauge precipitation data in the downscaling process partly enhances the

451   estimation accuracy. These methods highly rely on in situ measurements without the independence to rain gauge

452   measurements. In a recent hour scale downscaling study conducted by Ma et al. (2020), a geographically moving window

453   weight disaggregation analysis (GMWWDA) method was developed by introducing cloud properties as covariates to

454   downscale GPM precipitation. Although it provided estimates at a very high temporal frequency, the limited rainfall-

455   related environmental variables at the 0.01°/hourly scale constrained its application.

456   For the intercomparison of the monthly accuracy, the daily downscaled results of the proposed method

457   outperformed most of the previous monthly downscaling studies using either RF or GWR algorithms (Jing et al., 2016b;

458   Chen et al., 2018; Xu et al., 2015; Jia et al., 2011; Zhan et al., 2018). As shown in Figure 9b, the CC value was higher

459   than most of them in the abovementioned studies. Although the RF-based downscaling method in Jing et al. (2016b) has

460   a relatively low RMSE, the measurements from in situ stations were used to train the downscaling model which greatly

461   reduces the dependence of the downscaling process on field observations. A similar requirement is also presented in Lu

462   et al. (2019) and Long et al. (2016), and the GWR and multivariate regression models are largely dependent on the

463   number of available training stations and variables related to the geophysical mechanisms of precipitation. The

464   independence of field observations in the SMPD method shows a large advantage, especially for regions with sparse

465   meteorological stations. Zeng et al. (2021) also proposed an independent downscaling approach considering temporal

466   lag from vegetation changes to precipitation. However, the relationship shows high variability which may result in a

467   negative correlation within a short time. Therefore, both the CC and RMSE of this method have worse performances

468   than those of the proposed method. In general, according to the methodology comparison, the proposed SMPD method

469   exhibits good performance in terms of both CC and RMSE. Unlike using the empirical regression method to build the

470   relationship between precipitation and other surface variables, the SMPD method demonstrated high effectiveness,

471   independence, and robustness.

Table 2. List of the performance of downscaling procedures to improve the spatial resolution of satellite precipitation products at different temporal scales. The bold letters represent the proposed method in this study.

Original products	Downscaled algorithm	Auxiliary variables	Temporal resolution	Downscaled products			Reference
				Spatial resolution	CC	RMSE (mm)	
TRMM (25 km)	RF	DEM, NDVI	Monthly	1 km	0.86	15.70	Jing et al. (2016b)
GPM (10 km)	GWR	DEM, NDVI	Monthly	1 km	0.79	20.94	Lu et al. (2019)
GPM (10 km)	GWR	DEM, NDVI	Monthly	1 km	0.79	27.23	Zhan et al. (2018)
TRMM (25 km)	GWR	DEM, Rain gauge data	Monthly	1 km	0.87	46.14	Chen et al. (2018)
TRMM (25 km)	GWR	DEM, NDVI	Monthly	1 km	0.82	25.10	Xu et al. (2015)
GPM (10 km)	RF	DEM, NDVI, LST	Daily	1 km	0.64	6.06	Yan et al. (2021)
TRMM (25 km)	Multivariate regression model	DEM, Climate data	Daily	1 km	-	2.71	Long et al. (2016)
GPM (10 km)	LPVIAL	NDVI	16-day	1 km	0.81	46.77	Zeng et al. (2021)
CMORPH (8 km)	GWR	DEM, NDVI	30 min	1 km	0.86	7.27	Chao et al. (2018)
GPM (10 km)	GMWWDA	Cloud Property Data	Hourly	1 km	0.53	5.16	Ma et al. (2020)
GPM (10 km)	**SMPD**	**SSM, NDVI**	**Daily**	**1 km**	**0.61**	**4.83**	**Proposed method**

475   Despite the superior performance of the SMPD method, some issues still need to be considered in practical

476   applications. The first issue should relate to the accuracy of the original GPM precipitation data. Due to the limitation of

477   the inherent accuracy of original GPM precipitation data, the improvement in the accuracy of downscaling results is

478   limited because of the value preservation during the downscaling process. Therefore, the downscaling performance is

479   highly dependent on the accuracy of the original GPM. The multisource data fusion model based on observed stations

480   and reanalysis data proposed by Ma et al. (2021) and Li and Long (2020) could increase its ability to describe the daily

481   precipitation fluctuations and it would be helpful for providing more accurate downscaling precipitation values.

482   In addition, the responses of SSM with different land cover conditions and vegetation coverages to precipitation are

483   relatively different, and topographic factors such as depressions and slopes also affect the uncertainty of SSM. Therefore,

484   it is necessary to establish the relationship between SSM and precipitation for different land cover types or different

485   terrain types. The establishment of a more reliable fitting relationship based on precipitation data with different land

486   cover properties or topographic factors would be helpful to enhance the accuracy of the downscaling results (Senanayake

487   et al., 2021; Zhao et al., 2021; Chen et al., 2020). Furthermore, although the relationship between SSM and precipitation

488   has been well demonstrated in many previous studies, the sensitivity of SSM to precipitation will decrease when soil

489   water storage becomes saturated after repeated precipitation. Therefore, it is necessary to further improve the relationship

490   by considering the soil water threshold saturation in future studies. Moreover, this downscaling method was based on

491   the surface water balance principle, and the runoff factor under heavy precipitation conditions at a certain time was not

492   considered because of the inherent scarcity of high-resolution runoff datasets from in situ measurements. Some studies

493   have provided good alternatives to obtain runoff data with high spatiotemporal resolution (Jadidoleslam et al., 2019;

494   Muelchi et al., 2021). Hence, the use of this runoff factor in the water balance equation for heavy precipitation will assist

495   in improving downscaling accuracy.

496   **6 Conclusions**

497   In this paper, by introducing high-resolution SSM data and the NDVI as independent variables, a novel physical

498   downscaling approach based on the principle of surface water balance is developed to obtain high-resolution (1 km × 1

499   km) daily precipitation estimation. At both daily and monthly scales, the downscaled precipitation presents a similar

500   spatial and temporal distribution pattern as the original GPM product. Furthermore, a systematic evaluation of the

501   downscaled GPM data was conducted on multiple time scales at the station level. The downscaled precipitation showed

502   a good correlation with the observed measurements at each station at the daily scale, with FAR, CSI, CC, RMSE, and

503   BIAS values of 0.47, 0.48, 0.61, 4.83 mm, and 5%, respectively, and the evaluation results outperformed the original

504   GPM product. For monthly scale comparison, the downscaled data also presented a strong correlation with the observed

505   precipitation, with CC, RMSE, and BIAS values of 0.84, 30.88 mm, and 5%, respectively. With the increase in spatial

506   heterogeneity in the downscaled results, there is also an increasing trend in the improvements in the precipitation

507   accuracy through the comparison at most stations.

508   In summary, the proposed method with the use of surface water balance principle has a solider physical basis than

509   previous downscaling methods. Through introducing SSM as an auxiliary variable, the impact of inherent bias in satellite

510   estimates on the downscaled results can be moderately reduced compared to the conventional statistical method. The

511   validation with rain gauge data highlights the importance of SSM as a fully independent source of information that can

512   be effectively used for downscaling coarse-resolution precipitation at a daily scale, which is rarely conducted in current

513   related studies. Therefore, this method is a promising way to derive high-resolution precipitation data and shows good

514   potentials for real-time precipitation data downscaling with the provision of SSM data, which will assist further

515   applications in related fields (such as hydrology, agriculture, natural hazards, water resources, and climate change).

516   **Declaration of Competing Interest**

517   The authors declare that they have no known competing financial interests or personal relationships that could have

518   appeared to influence the work reported in this paper.

519   **Acknowledgments**

524   **References**

525   Baez-Villanueva, O. M., Zambrano-Bigiarini, M., Beck, H. E., McNamara, I., Ribbe, L., Nauditt, A., Birkel, C., Verbist, K., Giraldo-Osorio,

526   J. D., and Thinh, N. X.: RF-MEP: A novel Random Forest method for merging gridded precipitation products and ground-based

527   measurements, Remote Sensing of Environment, 239, 111606, 2020.

528   Bezak, N., Borrelli, P., and Panagos, P.: Exploring the possible role of satellite-based rainfall data to estimate inter-and intra-annual global

529   rainfall erosivity, Hydrology and Earth System Sciences Discussions, 1-27, 2021.

Hydrology and
Earth System
Sciences
Open Access
EGU
Discussions

530 Birtwistle, A. N., Laituri, M., Bledsoe, B., and Friedman, J. M.: Using NDVI to measure precipitation in semi-arid landscapes, Journal of
531   Arid Environments, 131, 15-24, https://doi.org/10.1016/j.jaridenv.2016.04.004, 2016.
532 Brocca, L., Moramarco, T., Melone, F., and Wagner, W.: A new method for rainfall estimation through soil moisture observations, Geophys.
533   Res. Lett., 40, 853-858, https://doi.org/10.1002/grl.50173, 2013.
534 Brocca, L., Filippucci, P., Hahn, S., Ciabatta, L., Massari, C., Camici, S., Schüller, L., Bojkov, B., and Wagner, W.: SM2RAIN–ASCAT
535   (2007–2018): global daily satellite rainfall data from ASCAT soil moisture observations, Earth Syst. Sci. Data, 11, 1583-1601,
536   10.5194/essd-11-1583-2019, 2019.
537 Brocca, L., Pellarin, T., Crow, W. T., Ciabatta, L., Massari, C., Ryu, D., Su, C. H., Rüdiger, C., and Kerr, Y.: Rainfall estimation by inverting
538   SMOS soil moisture estimates: A comparison of different methods over Australia, Journal of Geophysical Research Atmospheres, 121,
539   12,062-012,079, 2016.
540 Brocca, L., Ciabatta, L., Massari, C., Moramarco, T., Hahn, S., Hasenauer, S., Kidd, R., Dorigo, W., Wagner, W., and Levizzani, V.: Soil
541   as a natural rain gauge: Estimating global rainfall from satellite soil moisture data, J. Geophys. Res. - Atmos., 119, 5128-5141,
542   https://doi.org/10.1002/2014JD021489, 2014.
543 Brocca, L., Massari, C., Ciabatta, L., Moramarco, T., Penna, D., Zuecco, G., Pianezzola, L., Borga, M., Matgen, P., and Martínez-Fernández,
544   J.: Rainfall estimation from in situ soil moisture observations at several sites in Europe: an evaluation of the SM2RAIN algorithm,
545   Vodohospodársky časopis, 2015 v.63 no.3, pp. 201-209, 10.1515/johh-2015-0016, 2015.
546 Carpintero, E., Mateos, L., Andreu, A., and González-Dugo, M. P.: Effect of the differences in spectral response of Mediterranean tree
547   canopies on the estimation of evapotranspiration using vegetation index-based crop coefficients, Agr. Water Manage., 238, 106201,
548   https://doi.org/10.1016/j.agwat.2020.106201, 2020.
549 Chao, L., Zhang, K., Li, Z., Zhu, Y., Wang, J., and Yu, Z.: Geographically weighted regression based methods for merging satellite and
550   gauge precipitation, Journal of Hydrology, 558, 275-289, 2018.
551 Chen, F., Crow, W., and Holmes, T. R.: Improving long-term, retrospective precipitation datasets using satellite-based surface soil moisture
552   retrievals and the soil moisture analysis rainfall tool, Journal of Applied Remote Sensing, 6, 063604, 2012.
553 Chen, S., Xiong, L., Ma, Q., Kim, J.-S., Chen, J., and Xu, C.-Y.: Improving daily spatial precipitation estimates by merging gauge observation
554   with multiple satellite-based precipitation products based on the geographically weighted ridge regression method, J. Hydrol., 589,
555   125156, https://doi.org/10.1016/j.jhydrol.2020.125156, 2020.
556 Chen, Y., Huang, J., Sheng, S., Mansaray, L. R., Liu, Z., Wu, H., and Wang, X.: A new downscaling-integration framework for high-
557   resolution monthly precipitation estimates: Combining rain gauge observations, satellite-derived precipitation data and geographical
558   ancillary data, Remote Sens. Environ., 214, 154-172, https://doi.org/10.1016/j.rse.2018.05.021, 2018.
559 Ciabatta, L., Marra, A. C., Panegrossi, G., Casella, D., Sanò, P., Dietrich, S., Massari, C., and Brocca, L.: Daily precipitation estimation
560   through different microwave sensors: Verification study over Italy, J. Hydrol., 545, 436-450,
561   https://doi.org/10.1016/j.jhydrol.2016.12.057, 2017.
562 Ciabatta, L., Massari, C., Brocca, L., Gruber, A., Reimer, C., Hahn, S., Paulik, C., Dorigo, W., Kidd, R., and Wagner, W.: SM2RAIN-CCI:
563   a new global long-term rainfall data set derived from ESA CCI soil moisture, Earth Syst. Sci. Data, 10, 267-280, 10.5194/essd-10-267-
564   2018, 2018.
565 Colliander, A., Jackson, T. J., Bindlish, R., Chan, S., Das, N., Kim, S., Cosh, M., Dunbar, R., Dang, L., and Pashaian, L.: Validation of
566   SMAP surface soil moisture products with core validation sites, Remote Sensing of Environment, 191, 215-231, 2017.
567 Dorigo, W., Wagner, W., Albergel, C., Albrecht, F., Balsamo, G., Brocca, L., Chung, D., Ertl, M., Forkel, M., Gruber, A., Haas, E., Hamer,
568   P. D., Hirschi, M., Ikonen, J., de Jeu, R., Kidd, R., Lahoz, W., Liu, Y. Y., Miralles, D., Mistelbauer, T., Nicolai-Shaw, N., Parinussa,
569   R., Pratola, C., Reimer, C., van der Schalie, R., Seneviratne, S. I., Smolander, T., and Lecomte, P.: ESA CCI Soil Moisture for improved
570   Earth system understanding: State-of-the art and future directions, Remote Sens. Environ., 203, 185-215,
571   https://doi.org/10.1016/j.rse.2017.07.001, 2017.

572   Ebrahimy, H. and Azadbakht, M.: Downscaling MODIS land surface temperature over a heterogeneous area: An investigation of machine
573   learning techniques, feature selection, and impacts of mixed pixels, Computers & Geosciences, 124, 93-102,
574   https://doi.org/10.1016/j.cageo.2019.01.004, 2019.

575   Famiglietti, J. S. and Wood, E. F.: Multiscale modeling of spatially variable water and energy balance processes, Water Resour. Res., 30,
576   3061-3078, https://doi.org/10.1029/94WR01498, 1994.

577   Gruber, A., Scanlon, T., van der Schalie, R., Wagner, W., and Dorigo, W.: Evolution of the ESA CCI Soil Moisture climate data records
578   and their underlying merging methodology, Earth System Science Data, 11, 717-739, 2019.

579   Guo, X., Guo, Cui, P., Chen, X., Li, Y., Zhang, J., and Sun, Y.: Spatial uncertainty of rainfall and its impact on hydrological hazard
580   forecasting in a small semiarid mountainous watershed, J. Hydrol., 595, 126049, https://doi.org/10.1016/j.jhydrol.2021.126049, 2021.

581   Haylock, M. R., Cawley, G. C., Harpham, C., Wilby, R. L., and Goodess, C. M.: Downscaling heavy precipitation over the United Kingdom:
582   a comparison of dynamical and statistical methods and their future scenarios, International Journal of Climatology: A Journal of the
583   Royal Meteorological Society, 26, 1397-1415, 2006.

584   He, X., Chaney, N. W., Schleiss, M., and Sheffield, J.: Spatial downscaling of precipitation using adaptable random forests, Water resources
585   research, 52, 8217-8237, 2016.

586   Hou, A. Y., Kakar, R. K., Neeck, S., Azarbarzin, A. A., Kummerow, C. D., Kojima, M., Oki, R., Nakamura, K., and Iguchi, T.: The Global
587   Precipitation Measurement Mission, Bulletin of the American Meteorological Society, 95, 701-722, 10.1175/bams-d-13-00164.1, 2014.

588   Huffman, G. J., Bolvin, D. T., Braithwaite, D., Hsu, K., Joyce, R., Xie, P., and Yoo, S.-H.: NASA global precipitation measurement (GPM)
589   integrated multi-satellite retrievals for GPM (IMERG), Algorithm Theoretical Basis Document (ATBD) Version, 4, 26, 2015.

590   Huffman, G. J., Bolvin, D. T., Nelkin, E. J., Wolff, D. B., Adler, R. F., Gu, G., Hong, Y., Bowman, K. P., and Stocker, E. F.: The TRMM
591   Multisatellite Precipitation Analysis (TMPA): Quasi-global, multiyear, combined-sensor precipitation estimates at fine scales, Journal
592   of hydrometeorology, 8, 38-55, 2007.

593   Huffman, G. J., Adler, R. F., Arkin, P., Chang, A., Ferraro, R., Gruber, A., Janowiak, J., McNab, A., Rudolf, B., and Schneider, U.: The
594   global precipitation climatology project (GPCP) combined precipitation dataset, Bulletin of the American Meteorological Society, 78,
595   5-20, 1997.

596   Huffman, G. J., Bolvin, D. T., Braithwaite, D., Hsu, K.-L., Joyce, R. J., Kidd, C., Nelkin, E. J., Sorooshian, S., Stocker, E. F., and Tan, J.:
597   Integrated multi-satellite retrievals for the Global Precipitation Measurement (GPM) mission (IMERG), in: Satellite precipitation
598   measurement, Springer, Cham, 343-353, 2020.

599   Hutengs, C. and Vohland, M.: Downscaling land surface temperatures at regional scales with random forest regression, Remote Sens.
600   Environ., 178, 127-141, http://dx.doi.org/10.1016/j.rse.2016.03.006, 2016.

601   Immerzeel, W. W., Rutten, M. M., and Droogers, P.: Spatial downscaling of TRMM precipitation using vegetative response on the Iberian
602   Peninsula, Remote Sens. Environ., 113, 362-370, https://doi.org/10.1016/j.rse.2008.10.004, 2009.

603   Jadidoleslam, N., Mantilla, R., Krajewski, W. F., and Goska, R.: Investigating the role of antecedent SMAP satellite soil moisture, radar
604   rainfall and MODIS vegetation on runoff production in an agricultural region, Journal of Hydrology, 579, 124210,
605   https://doi.org/10.1016/j.jhydrol.2019.124210, 2019.

606   Jia, S., Zhu, W., Lü, A., and Yan, T.: A statistical spatial downscaling algorithm of TRMM precipitation based on NDVI and DEM in the
607   Qaidam Basin of China, Remote Sens. Environ., 115, 3069-3079, https://doi.org/10.1016/j.rse.2011.06.009, 2011.

608   Jing, W., Yang, Y., Yue, X., and Zhao, X.: A Spatial Downscaling Algorithm for Satellite-Based Precipitation over the Tibetan Plateau
609   Based on NDVI, DEM, and Land Surface Temperature, Remote Sens., 8, 655, 2016a.

610   Jing, W., Yang, Y., Yue, X., and Zhao, X.: A Comparison of Different Regression Algorithms for Downscaling Monthly Satellite-Based
611   Precipitation over North China, Remote Sensing, 8, 1-17, 2016b.

612   Joiner, J., Yoshida, Y., Anderson, M., Holmes, T., Hain, C., Reichle, R., Koster, R., Middleton, E., and Zeng, F.-W.: Global relationships
613   among traditional reflectance vegetation indices (NDVI and NDII), evapotranspiration (ET), and soil moisture variability on weekly
614   timescales, Remote Sens. Environ., 219, 339-352, https://doi.org/10.1016/j.rse.2018.10.020, 2018.

615   Joyce, R. J., Janowiak, J. E., Arkin, P. A., and Xie, P.: CMORPH: A method that produces global precipitation estimates from passive
616   microwave and infrared data at high spatial and temporal resolution, Journal of hydrometeorology, 5, 487-503, 2004.
617   Kubota, T., Shige, S., Hashizume, H., Aonashi, K., Takahashi, N., Seto, S., Hirose, M., Takayabu, Y. N., Ushio, T., and Nakagawa, K.:
618   Global precipitation map using satellite-borne microwave radiometers by the GSMaP project: Production and validation, IEEE
619   Transactions on Geoscience and Remote Sensing, 45, 2259-2275, 2007.
620   Li, X. and Long, D.: An improvement in accuracy and spatiotemporal continuity of the MODIS precipitable water vapor product based on
621   a data fusion approach, Remote Sensing of Environment, 248, 111966, 2020.
622   Lin, A. and Wang, X. L.: An algorithm for blending multiple satellite precipitation estimates with in situ precipitation measurements in
623   Canada, Journal of Geophysical Research: Atmospheres, 116, 2011.
624   Long, D., Bai, L., Yan, L., Zhang, C., Yang, W., Lei, H., Quan, J., Meng, X., and Shi, C.: Generation of spatially complete and daily
625   continuous   surface   soil   moisture   of   high   spatial   resolution,   Remote   Sens.   Environ.,   233,   111364,
626   https://doi.org/10.1016/j.rse.2019.111364, 2019.
627   Long, Y., Zhang, Y., and Ma, Q.: A Merging Framework for Rainfall Estimation at High Spatiotemporal Resolution for Distributed
628   Hydrological Modeling in a Data-Scarce Area, Remote Sensing, 8, 599, 2016.
629   Lu, X., Tang, G., Wang, X., Liu, Y., Jia, L., Xie, G., Li, S., and Zhang, Y.: Correcting GPM IMERG precipitation data over the Tianshan
630   Mountains in China, J. Hydrol., 575, 1239-1252, https://doi.org/10.1016/j.jhydrol.2019.06.019, 2019.
631   Ma, Y., Sun, X., Chen, H., Hong, Y., and Zhang, Y.: A two-stage blending approach for merging multiple satellite precipitation estimates
632   and rain gauge observations: An experiment in the northeastern Tibetan Plateau, Hydrology and Earth System Sciences, 25, 359-374,
633   2021.
634   Ma, Z., Xu, J., He, K., Han, X., Ji, Q., Wang, T., Xiong, W., and Hong, Y.: An updated moving window algorithm for hourly-scale satellite
635   precipitation   downscaling: A   case   study   in   the   Southeast   Coast   of   China,   J.   Hydrol.,   581,   124378,
636   https://doi.org/10.1016/j.jhydrol.2019.124378, 2020.
637   Mao, Y., Crow, W., and Nijssen, B.: A Framework for Diagnosing Factors Degrading the Streamflow Performance of a Soil Moisture Data
638   Assimilation System, Journal of Hydrometeorology, 20, 10.1175/JHM-D-18-0115.1, 2018.
639   Maraun, D., Wetterhall, F., Ireson, A., Chandler, R., Kendon, E., Widmann, M., Brienen, S., Rust, H., Sauter, T., and Themeßl, M.:
640   Precipitation downscaling under climate change: Recent developments to bridge the gap between dynamical models and the end user,
641   Reviews of geophysics, 48, 2010.
642   Maselli, F., Chiesi, M., Angeli, L., Fibbi, L., Rapi, B., Romani, M., Sabatini, F., and Battista, P.: An improved NDVI-based method to
643   predict   actual   evapotranspiration   of   irrigated   grasses   and   crops,   Agr.   Water   Manage.,   233,   106077,
644   https://doi.org/10.1016/j.agwat.2020.106077, 2020.
645   Massari, C., Brocca, L., Moramarco, T., Tramblay, Y., and Didon Lescot, J.-F.: Potential of soil moisture observations in flood modelling:
646   Estimating initial conditions and correcting rainfall, Adv. Water Resour., 74, 44-53, https://doi.org/10.1016/j.advwatres.2014.08.004,
647   2014.
648   McNally, A., Shukla, S., Arsenault, K. R., Wang, S., Peters-Lidard, C. D., and Verdin, J. P.: Evaluating ESA CCI soil moisture in East
649   Africa, Int. J. Appl. Earth Obs. Geoinf., 48, 96-109, https://doi.org/10.1016/j.jag.2016.01.001, 2016.
650   Mei, Y., Maggioni, V., Houser, P., Xue, Y., and Rouf, T.: A nonparametric statistical technique for spatial downscaling of precipitation over
651   High Mountain Asia, Water Resources Research, 56, e2020WR027472, 2020.
652   Merlin, O., Walker, J. P., Chehbouni, A., and Kerr, Y.: Towards deterministic downscaling of SMOS soil moisture using MODIS derived
653   soil evaporative efficiency, Remote Sens. Environ., 112, 3935-3946, 10.1016/j.rse.2008.06.012, 2008.
654   Mishra, V., Ellenburg, W. L., Griffin, R. E., Mecikalski, J. R., Cruise, J. F., Hain, C. R., and Anderson, M. C.: An initial assessment of a
655   SMAP soil moisture disaggregation scheme using TIR surface evaporation data over the continental United States, Int. J. Appl. Earth
656   Obs. Geoinf., 68, 92-104, https://doi.org/10.1016/j.jag.2018.02.005, 2018.
657   Mu, Q., Jones, L. A., Kimball, J. S., McDonald, K. C., and Running, S. W.: Satellite assessment of land surface evapotranspiration for the
658   pan-Arctic domain, Water Resour. Res., 45, https://doi.org/10.1029/2008WR007189, 2009.

659 Muelchi, R., Rssler, O., Schwanbeck, J., Weingartner, R., and Martius, O.: An ensemble of daily simulated runoff data (1981–2099) under
660   climate change conditions for 93 catchments in Switzerland (Hydro-CH2018-Runoff ensemble), Geoscience Data Journal, 2021.

661 Munsi, A., Kesarkar, A., Bhate, J., Panchal, A., Singh, K., Kutty, G., and Giri, R.: Rapidly intensified, long duration North Indian Ocean
662   tropical cyclones: Mesoscale downscaling and validation, Atmospheric Research, 259, 105678, 2021.

663 Nagler, P. L., Cleverly, J., Glenn, E., Lampkin, D., Huete, A., and Wan, Z.: Predicting riparian evapotranspiration from MODIS vegetation
664   indices and meteorological data, Remote Sens. Environ., 94, 17-30, https://doi.org/10.1016/j.rse.2004.08.009, 2005a.

665 Nagler, P. L., Scott, R. L., Westenburg, C., Cleverly, J. R., Glenn, E. P., and Huete, A. R.: Evapotranspiration on western U.S. rivers
666   estimated using the Enhanced Vegetation Index from MODIS and data from eddy covariance and Bowen ratio flux towers, Remote
667   Sens. Environ., 97, 337-351, https://doi.org/10.1016/j.rse.2005.05.011, 2005b.

668 Neinavaz, E., Skidmore, A. K., and Darvishzadeh, R.: Effects of prediction accuracy of the proportion of vegetation cover on land surface
669   emissivity and temperature using the NDVI threshold method, Int. J. Appl. Earth Obs. Geoinf., 85, 101984,
670   https://doi.org/10.1016/j.jag.2019.101984, 2020.

671 Pan, L., Xia, H., Zhao, X., Guo, Y., and Qin, Y.: Mapping Winter Crops Using a Phenology Algorithm, Time-Series Sentinel-2 and Landsat-
672   7/8 Images, and Google Earth Engine, Remote Sens., 13, 2510, 2021.

673 Peng, J., Loew, A., Zhang, S., Wang, J., and Niesel, J.: Spatial Downscaling of Satellite Soil Moisture Data Using a Vegetation Temperature
674   Condition Index, IEEE Trans. Geosci. Remote Sens., 54, 558-566, 10.1109/TGRS.2015.2462074, 2016.

675 Peng, J., Albergel, C., Balenzano, A., Brocca, L., Cartus, O., Cosh, M. H., Crow, W. T., Dabrowska-Zielinska, K., Dadson, S., Davidson,
676   M. W. J., de Rosnay, P., Dorigo, W., Gruber, A., Hagemann, S., Hirschi, M., Kerr, Y. H., Lovergine, F., Mahecha, M. D., Marzahn, P.,
677   Mattia, F., Musial, J. P., Preuschmann, S., Reichle, R. H., Satalino, G., Silgram, M., van Bodegom, P. M., Verhoest, N. E. C., Wagner,
678   W., Walker, J. P., Wegmüller, U., and Loew, A.: A roadmap for high-resolution satellite soil moisture applications – confronting product
679   characteristics with user requirements, Remote Sens. Environ., 252, 112162, https://doi.org/10.1016/j.rse.2020.112162, 2021.

680 Piles, M., Sanchez, N., Vall-llossera, M., Camps, A., Martinez-Fernandez, J., Martinez, J., and Gonzalez-Gambau, V.: A Downscaling
681   Approach for SMOS Land Observations: Evaluation of High-Resolution Soil Moisture Maps Over the Iberian Peninsula, IEEE J. Sel.
682   Topics Appl. Earth Observ. in Remote Sens., 7, 3845-3857, 10.1109/JSTARS.2014.2325398, 2014.

683 Prakash, S., Mitra, A. K., Pai, D. S., and AghaKouchak, A.: From TRMM to GPM: How well can heavy rainfall be detected from space?,
684   Advances in Water Resources, 88, 1-7, 10.1016/j.advwatres.2015.11.008, 2016.

685 Quiroz, R., Yarlequé, C., Posadas, A., Mares, V., and Immerzeel, W. W.: Improving daily rainfall estimation from NDVI using a wavelet
686   transform, Environ. modell. softw., 26, 201-209, https://doi.org/10.1016/j.envsoft.2010.07.006, 2011.

687 Rockel, B.: The regional downscaling approach: a brief history and recent advances, Current Climate Change Reports, 1, 22-29, 2015.

688 Rozante, J. R., Gutierrez, E. R., Fernandes, A. d. A., and Vila, D. A.: Performance of precipitation products obtained from combinations of
689   satellite and surface observations, International Journal of Remote Sensing, 41, 7585-7604, 2020.

690 Sabaghy, S., Walker, J. P., Renzullo, L. J., Akbar, R., Chan, S., Chaubell, J., Das, N., Dunbar, R. S., Entekhabi, D., Gevaert, A., Jackson, T.
691   J., Loew, A., Merlin, O., Moghaddam, M., Peng, J., Peng, J., Piepmeier, J., Rüdiger, C., Stefan, V., Wu, X., Ye, N., and Yueh, S.:
692   Comprehensive analysis of alternative downscaled soil moisture products, Remote Sens. Environ., 239, 111586,
693   https://doi.org/10.1016/j.rse.2019.111586, 2020.

694 Salzmann, M.: Global warming without global mean precipitation increase?, Science advances, 2, e1501572, 2016.

695 Senanayake, I. P., Yeo, I. Y., Willgoose, G. R., and Hancock, G. R.: Disaggregating satellite soil moisture products based on soil thermal
696   inertia: A comparison of a downscaling model built at two spatial scales, Journal of Hydrology, 594, 125894,
697   https://doi.org/10.1016/j.jhydrol.2020.125894, 2021.

698 Seneviratne, S. I., Corti, T., Davin, E. L., Hirschi, M., Jaeger, E. B., Lehner, I., Orlowsky, B., and Teuling, A. J.: Investigating soil moisture–
699   climate interactions in a changing climate: A review, Earth-Science Reviews, 99, 125-161,
700   http://dx.doi.org/10.1016/j.earscirev.2010.02.004, 2010.

701 Sheffield, J., Ferguson, C. R., Troy, T. J., Wood, E. F., and McCabe, M. F.: Closing the terrestrial water budget from satellite remote sensing,
702   Geophys. Res. Lett., 36, https://doi.org/10.1029/2009GL037338, 2009.

703   Shen, Y., Xiong, A., Hong, Y., Yu, J., Pan, Y., Chen, Z., and Saharia, M.: Uncertainty analysis of five satellite-based precipitation products
704   and evaluation of three optimally merged multi-algorithm products over the Tibetan Plateau, International journal of remote sensing,
705   35, 6843-6858, 2014.
706   Sorooshian, S., Hsu, K.-L., Gao, X., Gupta, H. V., Imam, B., and Braithwaite, D.: Evaluation of PERSIANN system satellite-based estimates
707   of tropical rainfall, Bulletin of the American Meteorological Society, 81, 2035-2046, 2000.
708   Spötl, C., Koltai, G., Jarosch, A., and Cheng, H.: Increased autumn and winter precipitation during the Last Glacial Maximum in the
709   European Alps, Nature communications, 12, 1-9, 2021.
710   Tagesson, T., Horion, S., Nieto, H., Zaldo Fornies, V., Mendiguren González, G., Bulgin, C. E., Ghent, D., and Fensholt, R.: Disaggregation
711   of SMOS soil moisture over West Africa using the Temperature and Vegetation Dryness Index based on SEVIRI land surface
712   parameters, Remote Sens. Environ., 206, 424-441, https://doi.org/10.1016/j.rse.2017.12.036, 2018.
713   Tang, G., Behrangi, A., Long, D., Li, C., and Hong, Y.: Accounting for spatiotemporal errors of gauges: A critical step to evaluate gridded
714   precipitation products, Journal of hydrology, 559, 294-306, 2018.
715   Tang, J., Niu, X., Wang, S., Gao, H., Wang, X., and Wu, J.: Statistical downscaling and dynamical downscaling of regional climate in China:
716   Present climate evaluations and future climate projections, Journal of Geophysical Research: Atmospheres, 121, 2110-2129, 2016.
717   Wehbe, Y., Temimi, M., and Adler, R. F.: Enhancing precipitation estimates through the fusion of weather radar, satellite retrievals, and
718   surface parameters, Remote Sensing, 12, 1342, 2020.
719   Wehbe, Y., Ghebreyesus, D., Temimi, M., Milewski, A., and Al Mandous, A.: Assessment of the consistency among global precipitation
720   products over the United Arab Emirates, Journal of Hydrology: Regional Studies, 12, 122-135, 2017.
721   Wei, K., Ouyang, C., Duan, H., Li, Y., Chen, M., Ma, J., An, H., and Zhou, S.: Reflections on the Catastrophic 2020 Yangtze River Basin
722   Flooding in Southern China, The Innovation, 1, 100038, https://doi.org/10.1016/j.xinn.2020.100038, 2020.
723   Wen, F., Zhao, W., Wang, Q., and Sánchez, N.: A Value-Consistent Method for Downscaling SMAP Passive Soil Moisture With MODIS
724   Products Using Self-Adaptive Window, IEEE Trans. Geosci. Remote Sens., 58, 913-924, 10.1109/TGRS.2019.2941696, 2020.
725   Xia, T., Wang, Z.-J., and Zheng, H.: Topography and Data Mining Based Methods for Improving Satellite Precipitation in Mountainous
726   Areas of China, Atmosphere, 6, 983-1005, 10.3390/atmos6080983, 2015.
727   Xu, S., Wu, C., Wang, L., Gonsamo, A., Shen, Y., and Niu, Z.: A new satellite-based monthly precipitation downscaling algorithm with
728   non-stationary relationship between precipitation and land surface characteristics, Remote Sens. Environ., 162, 119-140,
729   https://doi.org/10.1016/j.rse.2015.02.024, 2015.
730   Yan, X., Chen, H., Tian, B., Sheng, S., and Kim, J. S.: A Downscaling–Merging Scheme for Improving Daily Spatial Precipitation Estimates
731   Based on Random Forest and Cokriging, Remote Sensing, 13, 2040, 2021.
732   Yang, X. and Huang, P.: Restored relationship between ENSO and Indian summer monsoon rainfall around 1999/2000, The Innovation, 2,
733   100102, https://doi.org/10.1016/j.xinn.2021.100102, 2021.
734   Zeng, Z., Chen, H., Shi, Q., and Li, J.: Spatial Downscaling of IMERG Considering Vegetation Index Based on Adaptive Lag Phase, IEEE
735   Trans. Geosci. Remote Sens., 1-15, 10.1109/TGRS.2021.3070417, 2021.
736   Zhan, C., Han, J., Hu, S., Liu, L., and Dong, Y.: Spatial Downscaling of GPM Annual and Monthly Precipitation Using Regression-Based
737   Algorithms in a Mountainous Area, Advances in Meteorology, 2018, 1506017, 10.1155/2018/1506017, 2018.
738   Zhang, H., Ma, J., Chen, C., and Tian, X.: NDVI-Net: A fusion network for generating high-resolution normalized difference vegetation
739   index in remote sensing, ISPRS J. Photogramm. Remote Sens., 168, 182-196, https://doi.org/10.1016/j.isprsjprs.2020.08.010, 2020a.
740   Zhang, L., Ren, D., Nan, Z., Wang, W., Zhao, Y., Zhao, Y., Ma, Q., and Wu, X.: Interpolated or satellite-based precipitation? Implications
741   for hydrological modeling in a meso-scale mountainous watershed on the Qinghai-Tibet Plateau, Journal of Hydrology, 583, 124629,
742   https://doi.org/10.1016/j.jhydrol.2020.124629, 2020b.
743   Zhao, W., Sánchez, N., Lu, H., and Li, A.: A spatial downscaling approach for the SMAP passive surface soil moisture product using random
744   forest regression, J. Hydrol., 563, 1009-1024, https://doi.org/10.1016/j.jhydrol.2018.06.081, 2018.
745   Zhao, W., Wen, F., Wang, Q., Sanchez, N., and Piles, M.: Seamless downscaling of the ESA CCI soil moisture data at the daily scale with
746   MODIS land products, J. Hydrol., 603, 126930, https://doi.org/10.1016/j.jhydrol.2021.126930, 2021.